Band engineering in silicide alloys

Alexander Slepko and Alexander A. Demkov*
Department of Physics, University of Texas at Austin, Austin, Texas 78712, USA
(Received 8 June 2011; revised manuscript received 13 October 2011; published 12 January 2012)

A relatively low conductivity of PtSi is one of the impediments to its application as a contact material in semiconductor technology. In this paper, we discuss a possible strategy to control the conductivity of PtSi by manipulating the density of states at the Fermi level through alloying. Using density functional theory, we demonstrate theoretically that alloying PtSi with Ti substantially increases the number of conducting electrons and suggest possible ways to increase the Ti solubility limit. We identify a tertiary compound with the conducting electron concentration almost three times larger than that of bulk PtSi. We analyze the effect of Ti alloying on the work function of PtSi and its Schottky barrier height to Si, and we examine the effect of alloy scattering on PtSi conductivity.

DOI: 10.1103/PhysRevB.85.035311 PACS number(s): 71.55.Ak

I. INTRODUCTION

Continuous scaling of complementary metal oxide semiconductor devices drives the search for new metal silicide contact materials to the source, drain, and gate of a field effect transistor.[1] Typically, monosilicides are preferred over higher-order silicides, such as disilicides, due to a lower Si consumption. Nickel and platinum monosilicides have recently attracted significant interest.[2,3] Metal silicides are formed by heat treatment of a metal–semiconductor contact. Because of the formation mechanism, silicide–silicon interfaces are essentially free of contamination. Contacts formed in this manner generally show stable electrical characteristics, such as low line and contact resistance, and exhibit excellent mechanical adhesion.[4] Most importantly, however, the use of metal silicides allows the formation of self-aligning contacts, whereas in metallic conductors, their precise location usually depends on the fabrication process.

In this paper, using PtSi as an example, we employ first principles calculations to identify a strategy of improving electrical properties of silicide alloys via band engineering. The electronic structure and elastic constants of PtSi and Pt_2Si were previously investigated theoretically using density functional theory.[5–7] Our group has reported theoretical studies of the surface energy and work function (WF) of bulk PtSi[8] and the electronic, optical, and surface properties of PtSi thin films.[9] PtSi is attractive because of its relatively low (0.2 eV) Schottky barrier to the valence band of Si (001) and excellent thermal stability.[10] However, as a contact material, PtSi suffers from relatively low conductivity (e.g., when compared with Pt), which can be traced to the low electronic density of states (DOS) at the Fermi level in bulk PtSi. A look at the PtSi DOS (Fig. 1) reveals that the Fermi level "misses" the high DOS region corresponding to Pt *d* states. A naïve integration of the electronic DOS suggests that in a unit cell of bulk PtSi, ∼7.5 electrons need to be removed to shift the Fermi level down in energy toward the high DOS region of the spectrum. To achieve this, we suggest doping PtSi with Ti substitutionally on the Pt site. Both PtSi and TiSi monosilicides can be stabilized in a primitive orthorhombic structure with space group *Pnma* (No. 62 in the International X-Ray Tables), where PtSi crystallizes in a MnP-type lattice and TiSi in a FeB-type lattice, as shown in Figs. 2(a) and 2(b), respectively. Moreover, Ti and Pt atoms are almost equal in size (the atomic radius of Ti of 1.4 Å is only 5% larger than that of Pt), but Ti contributes only 4 electrons per atom to the total amount of valence electrons, versus the 10 electrons per atom contributed by Pt. In a primitive unit cell of PtSi, this means that 1.25 out of 4 Pt atoms need to be replaced by Ti. We test this idea by means of first principles density functional theory calculations. Our calculations suggest that Ti doping may result in a significant increase of the DOS at the Fermi level, followed by an increase in the number of conducting electrons (those in the interval $-k_BT + E_F \leqslant E \leqslant k_BT + E_F$). We predict an increase of up to 2.7 times in the number of conducting electrons compared to bulk PtSi. Importantly, we find that on average, the Schottky barrier to Si is rather insensitive to Ti doping. Using a simple ideal mixture theory to estimate the entropic effect of mixing, we find the solubility limit of Ti in bulk PtSi (on the Pt site) at 500 K to be ∼0.5 at.%. Unfortunately, this is not sufficient to realize the gains in the electron density in practice. To circumvent this problem, we find that additional alloying with gallium or aluminum can significantly increase the solubility limit of Ti in PtSi. We also estimate the effect of alloy scattering on the conductivity.

The rest of the paper is organized as follows. We summarize computational details in Sec. II. In Sec. III, we discuss the electronic structure of $Ti_xPt_{1-x}Si$ alloys, estimate the carrier density, and analyze the effect of Ti doping on the WF and Schottky barrier height (SBH) with Si (001). Using Boltzmann transport formalism, we calculate the change in conductivity due to introduced Ti impurity scattering. In Sec. IV, we discuss the solubility limit of Ti in bulk PtSi and consider possible routes to increase the solubility limit of Ti via stabilizing $Ti_xPt_{1-x}Si$ alloys by additional doping with boron, carbon, gallium, and aluminum.

II. COMPUTATIONAL DETAILS

All calculations are done using density functional theory within the local density approximation and ultrasoft pseudopotentials,[12] as included in the Vienna *ab initio* simulation package (VASP) code.[13–17] We use the valence configurations ($3d^3$, $4s^1$) for titanium, ($6s^1$, $5d^9$) for platinum, and ($3s^2$, $3p^2$) for silicon. The 300-eV kinetic energy cutoff

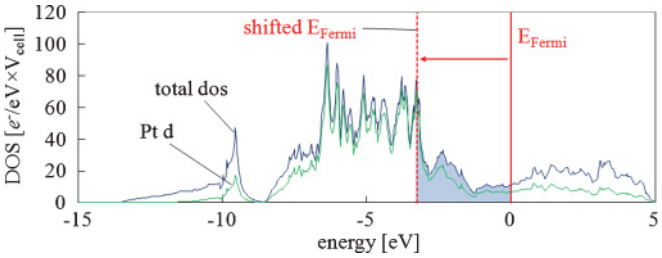

FIG. 1. (Color online) DOS of bulk PtSi in a $2 \times 2 \times 2$ supercell. The zero of energy is set to the Fermi level. The arrow indicates how the Fermi level has to be moved to a hypothetical energy (dashed line) to provide a large carrier concentration accessible for electrical conductivity.

yields 1 meV/cell convergence for bulk PtSi. To investigate the effects of doping with Ti on the DOS and number of carriers at the Fermi level for different Ti concentrations, we consider $2 \times 2 \times 6$, $2 \times 2 \times 3$, $2 \times 2 \times 2$, $2 \times 1 \times 2$, and $1 \times 2 \times 2$ supercells and the primitive cell. For the Brillouin zone integration of these cells, we use the following Monkhorst-Pack[18] k-point meshes: $4 \times 4 \times 2$, $4 \times 4 \times 4$, $4 \times 4 \times 6$, $8 \times 14 \times 12$, $14 \times 8 \times 12$, and $13 \times 13 \times 17$. All structures are optimized

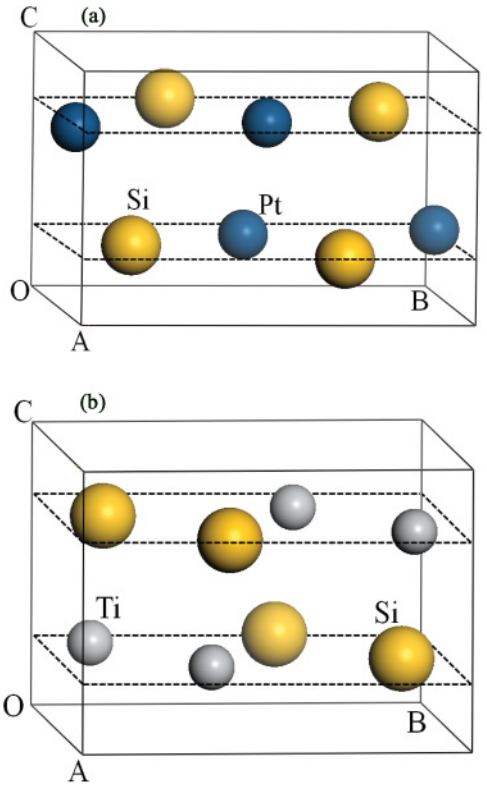

FIG. 2. (Color online) (a) Primitive cell of bulk PtSi. PtSi crystallizes in the primitive orthorhombic structure with a MnP-type lattice with space group *Pnma* (No. 62 in the International X-Ray Tables). The lattice constants are $a = 5.922$ Å, $b = 5.575$ Å, and $c = 3.586$ Å (Ref. 11). The smaller balls are Pt, and the bigger balls are Si atoms. The exact positions of all atoms are summarized in Table II. (b) Primitive cell of bulk TiSi. TiSi crystallizes in the primitive orthorhombic structure with a FeB-type lattice with space group *Pnma*. The lattice constants are $a = 6.544$ Å, $b = 4.997$ Å, and $c = 3.638$ Å.

with respect to ionic positions, cell shape, and volume until the forces on all atoms are less than 20 meV/Å. The energy is converged to 10^{-3} meV/cell. The relaxation is not constrained by symmetry.

We consider $Ti_xPt_{1-x}Si$ and Ti_xPtSi_{1-x} alloys with 0.52, 1.04, 1.56, 3.13, 6.25, and 12.5 at.% Ti substitution. For the two lowest concentrations, we use the $2 \times 2 \times 6$ and $2 \times 2 \times 3$ supercells of PtSi (in each case, we replace only one Pt atom with Ti). We use a $2 \times 2 \times 2$ supercell of PtSi for the Ti concentrations of 1.56 and 3.13 at.%, where 1 and 2 out of the 32 Pt atoms are substituted with Ti. We analyze all 31 possibilities to substitute two Pt atoms with Ti (3.13 at.%). Alloys with 6.25 at.% Ti can be realized using $2 \times 2 \times 2$ supercells of PtSi, where four Pt atoms are replaced by Ti. That yields 4495 possibilities to arrange the Ti atoms in the cell. With 12.5 at.% Ti (eight atoms in a $2 \times 2 \times 2$ supercell), there are 2 629 575 possibilities. Because such a large number of calculations is not realizable, we analyze smaller $2 \times 1 \times 2$ and $1 \times 2 \times 2$ supercells for 6.25 at.% Ti. In each case, that yields 15 structures with the Ti concentration of 6.25 at.% (including symmetrically equivalent structures). In alloys with 12.5 at.% Ti, we limit our studies to a primitive cell of PtSi and replace one Pt atom with Ti, resulting in only one possible structure. For this high concentration, in principle we could use a bigger simulation cell with a quasirandom distribution of Ti; however, the solubility limit makes this case difficult to realize in practice. To calculate the WF and SBH, we use slab geometry with simulation cells of the size $\sim 10 \times 10 \times 45$ Å (the side lengths vary slightly depending on the models used, as described later), along with a $4 \times 4 \times 2$ Monkhorst-Pack k-point mesh for Brillouin zone integration.

III. ELECTRONIC AND THERMODYNAMIC PROPERTIES OF $Ti_xPt_{1-x}Si$ ALLOYS

A. Influence of Ti doping on the DOS

The high DOS at the Fermi level is one of the main requirements for having high electrical conductivity. By integrating the DOS within the $2k_BT$ energy window around the Fermi level (e.g., at $T = 300$ K) the carrier density n can be determined. To analyze the effect of Ti doping on the DOS and n, we consider Ti concentration of 0.52, 1.04, 1.56, 3.13, 6.25, and 12.5 at.%. For concentrations of 3.13 and 6.25 at.%, we consider 61 possible Pt substitutions in total. Here, we only focus on the most stable configurations. Our results for the DOS at the Fermi level and the carrier density n are summarized in Table I. For comparison, we included the results for Ti substitution of Si. As expected, the effect on the carrier concentration is minimal. In Fig. 3, we show the DOS of $Ti_xPt_{1-x}Si$ for the Ti concentrations of 1.56, 3.13, 6.25, and 12.5 at.%. Contrary to our original intention to shift the Fermi level toward the region of high density of Pt d states, we find that it moves little yet produces a noticeable change in the number of states at the Fermi level. Figure 4 (the partial DOS of the alloy with 12.5 at.% Ti) shows that the increase is due to the introduction of Ti d states that appear just above the d states of Pt in energy (the energy difference of the atomic d-levels is $E_{Ti-d} - E_{Pt-d} \approx 5.42$ eV[19]), rather than to a shift of the Fermi energy. Therefore, though the "rigid band" assumption has

TABLE I. DOS at the Fermi level and carrier density in $Ti_xPt_{1-x}Si$ and Ti_xPtSi_{1-x} alloys for different Ti concentrations. The DOS is given per 2 × 2 × 2 cell. For Ti concentrations higher than 1 at.%, we observe an increase in both DOS and carrier density for doping on either site.

	Ti on Pt site			Ti on Si site		
Ti (at.%)	DOS at E_F (electron/eV × V_{Cell})	n (10^{20} electron/cm^3)	T_{crit} (K)	DOS at E_F (electron/eV × V_{Cell})	n (10^{20} electron/cm^3)	T_{crit} (K)
0.00	14.5	7.9	0	14.5	7.9	0
0.52	14.9	7.7	0	13.2	6.6	1814
1.04	15.1	8.6	879	16.6	9.2	1508
1.56	15.9	9.1	905	14.8	8.6	1337
3.13	18.0	9.4	1532	13.5	7.6	618
6.25	17.0	13.8	2809			
12.50	25.2	21.5	3618			

proved to be an oversimplification, we find that doping with Ti increases the number of carriers in PtSi. We also find that substituting Si with Ti does not affect the carrier concentration significantly. Later, we analyze the thermodynamic stability of Si- and Pt-substituted TiPtSi alloys.

B. Influence of Ti doping on the WF and SBH

One of the key characteristics of any contact material is its SBH to Si. Thus, it is important to understand how Ti doping may affect the barrier height. We start by considering the effect of doping on the WF φ_m of PtSi, which is defined as a difference between the vacuum energy in the immediate vicinity of its surface and the Fermi level. To simulate the silicide surface, we use slab geometry. The thickness of the $Ti_xPt_{1-x}Si$ slab is ∼25 Å, and it is followed by 15 Å of vacuum to minimize the slab–slab interaction introduced through the periodic boundary conditions. We calculate the local electrostatic potential of the cell and average it over the x–y plane along the z-axis (direction normal to the surface). A typical plot of this planar-averaged local potential is shown in Fig. 5(a). We approximate the vacuum energy level with the value of the electrostatic potential in the vacuum region of the simulation cell. The WF is then easily extracted. We compare the WF of $Ti_xPt_{1-x}Si$ with 3.13 at.% Ti (Ti on Pt site) to the bulk PtSi for the surface orientations (001), (010), (100), (101), (011), and (110). We consider three surface terminations (Pt, Si, and Ti

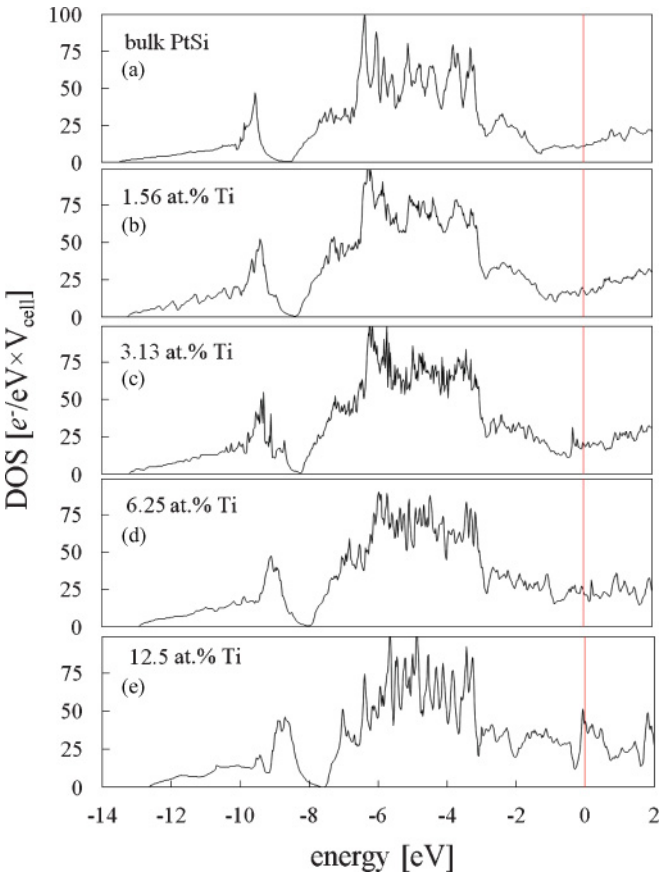

FIG. 3. (Color online) DOS of (a) bulk PtSi, (b) $TiPt_{31}Si_{32}$, (c) $Ti_2Pt_{30}Si_{32}$, (d) $Ti_4Pt_{28}Si_{32}$, and (e) $Ti_8Pt_{24}Si_{32}$ corresponding to 0, 1.56, 3.13, 6.25, and 12.5 at.% Ti, respectively. E_F is at 0. The DOS is calculated with respect to a 2 × 2 × 2 cell of bulk PtSi.

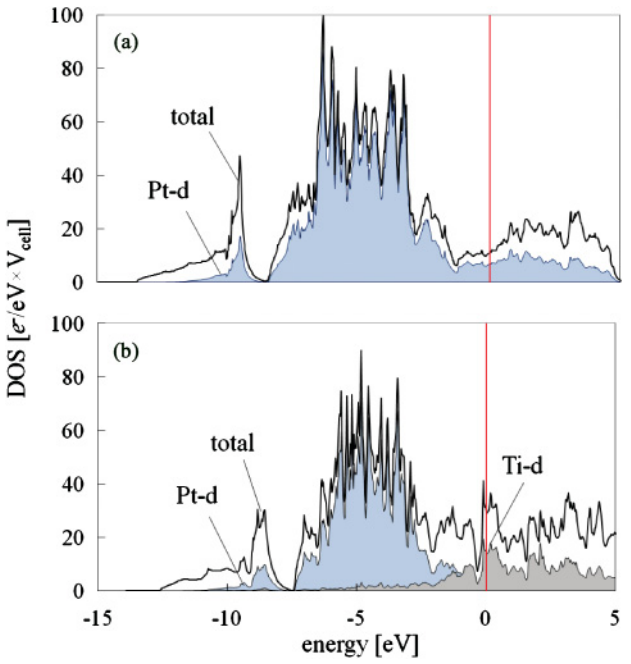

FIG. 4. (Color online) Total DOS and d states of (a) bulk PtSi and (b) $Ti_8Pt_{24}Si_{32}$ (12.5 at.% Ti). The zero of energy is set to the Fermi level. The Ti d states appear at the Fermi level, thus increasing the carrier concentration considerably from that of PtSi.

TABLE II. Experimental and theoretical internal in-plane coordinates in the orthorhombic *Pnma* cell of PtSi. Pt atoms are located at $[u_{\mathrm{Pt}}, v_{\mathrm{Pt}}, 1/4]$, $[1/2 - u_{\mathrm{Pt}}, v_{\mathrm{Pt}} - 1/2, 1/4]$, $[1 - u_{\mathrm{Pt}}, 1 - v_{\mathrm{Pt}}, 3/4]$, and $[1/2 + u_{\mathrm{Pt}}, 3/2 - v_{\mathrm{Pt}}, 3/4]$, whereas Si atoms are located at $[u_{\mathrm{Si}}, v_{\mathrm{Si}}, 1/4]$, $[3/2 - u_{\mathrm{Si}}, 1/2 + v_{\mathrm{Si}}, 1/4]$, $[u_{\mathrm{Si}} - 1/2, 1/2 - v_{\mathrm{Si}}, 3/4]$, and $[1 - u_{\mathrm{Si}}, 1 - v_{\mathrm{Si}}, 3/4]$. The positions are given in fractional coordinates.

	u_{Pt}	v_{Pt}	u_{Si}	v_{Si}	Ref.
Experiment	0.1922	0.9956	0.583	0.177	11
Theory	0.1920	0.9980	0.585	0.178	This work

termination), as depicted in Fig. 6 for the (100) surface. For the (001) orientation, a stoichiometric surface is constructed, because cleaving in this direction always yields a surface with an equal amount of Pt and Si in the surface plane rather than Pt or Si rumpling out of it (as is the case for all other orientations). Our results are summarized in Table III and plotted in Fig. 7. First, with the exception of the Si-terminated (010) surface, Ti slightly increases the WF compared to equivalent PtSi surfaces. Second, with the exception of the (101) orientation, Ti-terminated surfaces always have a lower WF than PtSi surfaces with the same orientation and any termination. The highest difference (0.45 eV) is found for the (010) surface when comparing the Ti-terminated $\mathrm{Ti}_x\mathrm{Pt}_{1-x}\mathrm{Si}$ with Pt-terminated PtSi. This can be traced to Ti 3*d* states being higher in energy than the *d* states of Pt. Within the Schottky model, these changes in the WF should greatly influence the barrier height between the metal's Fermi level and the semiconductor's

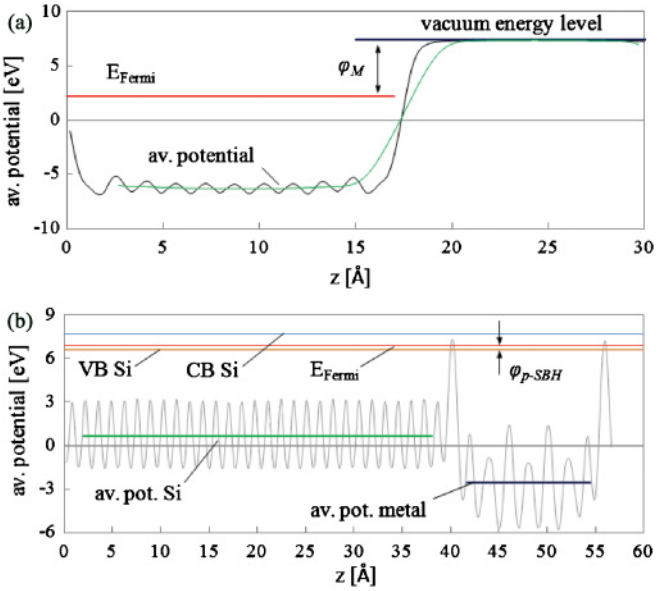

FIG. 5. (Color online) (a) Local potential and planar-averaged local potential of a (100) $\mathrm{Ti}_x\mathrm{Pt}_{1-x}\mathrm{Si}$ surface. The difference in energy between the vacuum level and the highest occupied level in the metal (i.e., the Fermi level) is the WF of the calculated surface. (b) Local potential and planar-averaged potential of a (001)/(110) $\mathrm{Ti}_x\mathrm{Pt}_{1-x}\mathrm{Si}$/Si interface. Indicated also are the top of the valence band and the bottom of the conduction band of the Si bulk. The difference between the top of the valence band and the Fermi level of the system is the *p*-type SBH.

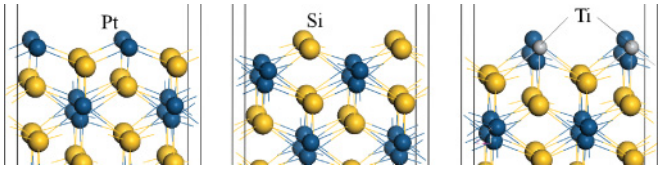

FIG. 6. (Color online) Surface models with Si termination (Si on top of the surface), Pt termination, and a termination with Ti atoms at the surface. All surfaces shown are (100) oriented.

valence or conduction bands. In the following, we analyze two theoretical silicide/Si interface models to gain insight in the dependence of the SBH on Ti doping.

The SBH of a metal to a *p*-type semiconductor is defined as the energy difference between the top of the valence band of the semiconductor and the Fermi level of the metal,

$$\varphi_p = E_{VB} - \varphi_m, \tag{1}$$

where E_{VB} is the energy of the semiconductor's valence band top with respect to the vacuum level and φ_m is the metal WF. Conversely, the *n*-type SBH is the energy difference between the Fermi level of the metal and the bottom of the conduction band of the semiconductor.

To estimate the effect of Ti doping on the SBH, we construct two model interfaces—Si(001)/$\mathrm{Ti}_x\mathrm{Pt}_{1-x}$Si(001) and Si(001)/$\mathrm{Ti}_x\mathrm{Pt}_{1-x}$Si(110)—using superlattice geometry. We calculate the SBH for 0 and 3.13 at.% Ti while substituting Ti at the interface directly as that yields the largest change in the WF. The ∼35-Å-thick Si slab is used as a substrate; i.e., the silicide layers are laterally lattice matched to it. The silicide is ∼15 Å thick. The substrate and metal are initially separated by 1.8 Å (determined by a quadric fit of the binding energy). The lateral dimensions are 11.5 × 11.5 and 7.6 × 15.3 Å in our (001)/(001) and (110)/(001) models, respectively. We apply 3.0 × −2.9 and 6.2 × −5.9 % lateral strain to the metal

TABLE III. Theoretical WFs for $\mathrm{Ti}_x\mathrm{Pt}_{1-x}\mathrm{Si}$ with 3.13 at.% Ti and bulk PtSi. Ti-terminated surfaces have a lower WF compared to the corresponding PtSi surfaces, with the exception of the (101) orientation.

		φ (eV)	
(hkl)	Termination	$\mathrm{Ti}_x\mathrm{Pt}_{1-x}\mathrm{Si}$	PtSi
001	stoichiometric	5.28	5.22
	Ti	5.14	
010	Pt	5.40	5.39
	Si	5.10	5.24
	Ti	4.94	
100	Pt	5.11	5.11
	Si	5.02	5.02
	Ti	4.73	
101	Si	5.15	5.03
	Ti	5.25	
011	Pt	5.23	5.18
	Si	5.26	5.12
	Ti	5.00	
110	Pt	5.06	4.96
	Si	5.35	5.29
	Ti	4.88	

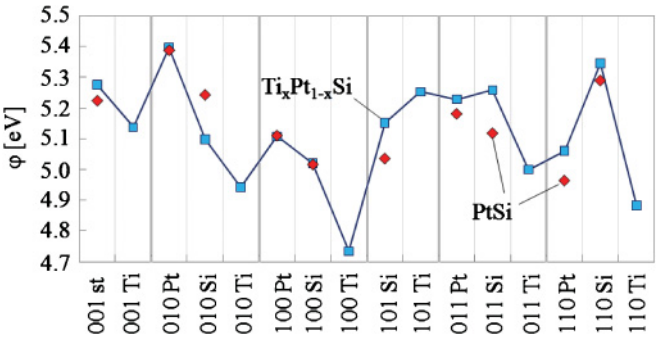

FIG. 7. (Color online) Calculated WFs of PtSi (diamonds) and $Ti_xPt_{1-x}Si$ alloys (squares). The (101) orientation of the WF of $Ti_xPt_{1-x}Si$ decreases by up to ~0.5 eV compared to that of PtSi.

layers to match them with the Si substrate and relax the ionic positions while keeping the lattice constants and simulation cell shape constant. After relaxation, the residual stress is less than 0.6 GPa in the (001)/(001) model and less than 1 GPa in the (001)/(110) model.

We extract the *p*-type SBH from the calculated local electrostatic potential. Again, the potential is averaged over the x–y plane for each z value. A typical plot of the planar-averaged local potential is shown in Fig. 5(b). Deep inside the Si and metal regions, we expect to find bulklike conditions in both materials. Within the bulk regions, the planar-averaged microscopic potential is also macroscopically averaged along the z-axis. The top of the valence band of Si in the bulk region is placed with respect to the averaged potential in the Si slab using a separate bulk calculation. The SBH is then easily extracted, as shown in Fig. 5(b). Our results are summarized in Table IV. For our (001)/(001) model, we find a SBH of 0.13 eV for both PtSi and $Ti_xPt_{1-x}Si$. For our (110)/(001) model, we find 0.11 and 0.08 eV for PtSi and $Ti_xPt_{1-x}Si$ contacts, respectively. The calculated barrier heights for PtSi contacts are in fair agreement with our previously reported value of 0.16 eV for the PtSi(001)/Si(001) interface,[8] where a smaller cell (higher stress) was used to reduce the computational time. It is somewhat smaller than the experimental value of 0.2 eV.[10]

Equation (1) suggests a linear increase in the SBH for decreasing WF. Although in the previous section we found that Ti doping reduces the WF of PtSi by ~0.1 eV for the (001) and (110) Ti-terminated surfaces, our calculated barrier heights are rather insensitive to this change. To gain more insight, we apply the metal-induced gap states (MIGS) theory[20] for SBHs and compare with our results:

$$\varphi_p = E_g - S \times (\varphi_m - \varphi_{\mathrm{CNL}}) - (\varphi_{\mathrm{CNL}} - \chi). \qquad (2)$$

Here, E_g is the band gap of the semiconductor (1.1 eV for Si), φ_m is the metal WF, φ_{CNL} is the charge neutrality level (CNL) of the semiconductor, and χ is its electron affinity. The pinning parameter S is believed to be an intrinsic property of the semiconductor surface. In the Schottky limit ($S = 1$, i.e., no Fermi level pinning), Eq. (2) gives "maximum dependence" on the WF. In the Bardeen limit ($S = 0$, i.e., strong Fermi level pinning), the SBH does not depend on the metal WF. Equation (2) is a linear interpolation between the Schottky and the Bardeen limits. In practice, S can be approximated by[21]

$$S = \frac{1}{1 + 0.1 \times (\varepsilon_\infty - 1)^2}, \qquad (3)$$

where ε_∞ is the high frequency limit of the dielectric constant of Si. Using $\varepsilon_\infty = 11.7$, the pinning parameter of Si is 0.08, indicating little dependence of the SBH on the WF. According to Bardeen, the CNL is the intrinsic property of the material and is essentially the Fermi level at the surface. In the literature, theoretical values of the Si CNL vary between ~0.3 and ~0.36 eV above the valence band top, somewhat depending on the method of calculation.[22–24] For a CNL of 0.3 eV above the valence band top and electron affinity of 4.1 eV[25] in the Bardeen or strong pinning limit, the SBH is always 0.30 eV. In the Schottky limit, the barrier height averaged over our (001)/(001) and (110)/(001) models is 0.13 eV for PtSi/Si interfaces. For our $Ti_xPt_{1-x}Si$/Si interfaces, it is 0.21 eV—0.08 eV higher than for the PtSi/Si interfaces. This shift reflects the linear dependence of the SBH on the change in WF in the Schottky limit. However, our calculations indicate the difference between the SBH of $Ti_xPt_{1-x}Si$/Si and that of PtSi/Si interfaces of only 0.01 eV, suggesting little dependence of the SBH on the metal WF. Thus, our results are in qualitative agreement with the Bardeen model, i.e., the change in the WF does not influence the SBH, as reflected by a small value of the pinning parameter S.

C. Impurity scattering in $Ti_xPt_{1-x}Si$ alloys

Thus far, we have demonstrated that doping PtSi with Ti can increase the number of carriers without significantly altering the Schottky barrier to Si. However, doping typically is accompanied by an increase in scattering that may adversely affect mobility. To analyze the change in carrier mobility with increasing Ti concentration in bulk PtSi, we use Boltzmann transport formalism.[26,27] Assuming that collisions of electrons with substitutional Ti atoms are elastic and spin conserving, we can calculate the collision term in the Boltzmann equation and estimate the change in carrier mobility of a system due

TABLE IV. Comparison of the SBHs extracted from local potential plots with MIGS theory and Bardeen and Schottky models. The Ti concentration in the $Ti_xPt_{1-x}Si$ alloys is 3.13 at.%. BL stands for Bardeen limit and SL stands for Schottky limit.

Interface	VASP SBH (eV)		MIGS SBH (eV)		BL (eV)		SL (eV)	
(metal/Si)	PtSi	TiPtSi	PtSi	TiPtSi	PtSi	TiPtSi	PtSi	TiPtSi
001/001	0.13	0.13	0.28	0.28			0.00	0.08
110/001	0.11	0.08	0.30	0.30	0.30	0.30	0.26	0.34
001/001[a]	0.16		0.29					

[a]Ultra soft. pseudopotentials (Ref. 8).

to impurities. Similar calculations were recently performed by Evans *et al.*, who analyzed the channel mobility degradation in a field effect transistor caused by interface defects.[28]

To calculate the probability for an electron in band n with the wave vector $\vec{k}$ to scatter into band m with the wave vector $\vec{k}'$, we compute the impurity scattering potential ΔV and its scattering matrix element,

$$T_{mn}(\vec{k}',\vec{k}) = \langle n\vec{k}|\Delta V|m\vec{k}'\rangle, \tag{4}$$

where the unperturbed wave functions $|m\vec{k}'\rangle$ and $|n\vec{k}\rangle$ are the Bloch states of undoped PtSi normalized to unity; i.e., the absolute square of the wave function integrated over the primitive cell equals 1. The impurity scattering potential ΔV is calculated from first principles within density functional theory by subtracting the local potentials computed for a simulation cell of PtSi and $Ti_xPt_{1-x}Si$. Due to the metallic nature of PtSi, the perturbation $|\Delta V|$ is short ranged and the integration in Eq. (4) can be reduced to an integral over the simulation cell, provided it is sufficiently large. To ensure that the potential is fully contained in the simulation cell, we calculate carrier mobility in a $2 \times 2 \times 2$ cell with one Ti impurity. In our approach, we only relax the ionic positions in the perturbed and unperturbed cells, keeping the cell shape and volume fixed. The impurity potential is shown in Fig. 8 in the form of cross-sectional contour plots in three orthogonal planes containing the impurity site. It ranges between -15 and 15 eV and is roughly on the order of the kinetic energy of the fastest electron whose band velocity is 16 Å/fs (Fig. 9). The peak energy values of the potential are contained within a sphere with a radius of ~3 Å around the Ti impurity; thus, it is well contained in the simulation cell.

Using Eq. (4) and the Fermi golden rule, we calculate the rate of scattering from state $|m\vec{k}'\rangle$ to state $|n\vec{k}\rangle$,

$$\Gamma_{mn}(\vec{k}',\vec{k}) = \frac{2\pi}{\hbar} \times n_d \times V \times |T_{mn}(\vec{k}',\vec{k})|^2 \delta(E_n(\vec{k}) - E_m(\vec{k}')), \tag{5}$$

where n_d is the impurity density, V is the volume of the simulation cell, and $E_n(\vec{k})$ and $E_m(\vec{k}')$ are the energy eigenvalues of the unperturbed wave functions $|n\vec{k}\rangle$ and $|m\vec{k}'\rangle$. The total rate is then obtained by summing over the first Brillouin zone, multiplied by the probability for the initial state to be filled and the final state to be empty, and subtracting the rates of backscattered carriers. The inverse scattering time for a state $|n\vec{k}\rangle$ is then given by

$$\frac{1}{\tau_n(\vec{k})} = \sum_{m,\vec{k}'} \Gamma_{mn}(\vec{k}',\vec{k})(1 - \cos(\Theta_{\vec{k},\vec{k}'})), \tag{6}$$

where the sum only runs over states within the range $-k_BT + E_F \leqslant E \leqslant E_F + k_BT$, because only these states contribute to scattering.

In Eq. (5), the δ-function ensures energy conservation. In practice, we replace the δ-function by a properly normalized window function. Then, scattering is only possible for states satisfying $|E_n(\vec{k}) - E_m(\vec{k}')| < \varepsilon$. The width of the window function is 2ε. In our study, we use the value $\varepsilon = 10$ meV (the difference between using this and using $\varepsilon = 15$ meV in the later calculated mobility is within 5%). Carrier mobility is given by[27]

$$\mu_{\alpha\beta} = -e \sum_{n,\vec{k}} \tau_n(\vec{k})[\vec{v}_n(\vec{k})]_\alpha [\vec{v}_n(\vec{k})]_\beta \frac{\partial f_0(E_n(\vec{k}))}{\partial E}. \tag{7}$$

In Eq. (7), the function $f_0(E_n(\vec{k}))$ is the equilibrium Fermi-Dirac distribution with the chemical potential set to the Fermi

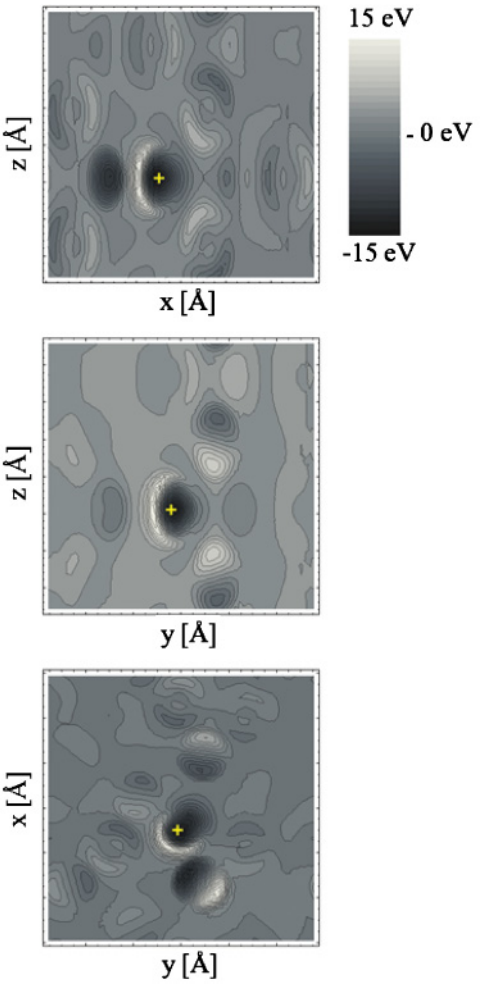

FIG. 8. (Color online) Contour plots of the scattering potential of a Ti impurity in a $2 \times 2 \times 2$ cell of bulk PtSi. The Ti is placed substitutionally on a Pt site. The position of the impurity is indicated by the cross. The impurity potential varies from -15 to 15 eV.

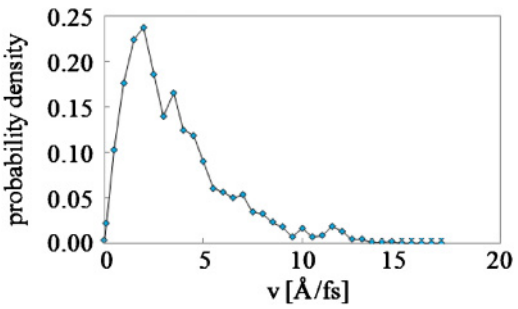

FIG. 9. (Color online) Distribution of band velocities within $\pm k_BT$ at room temperature around the Fermi level. The highest calculated velocity is 16 Å/fs. The distribution peaks at 2 Å/fs.

TABLE V. Carrier mobility and conductivity tensors of $Ti_xPt_{1-x}Si$ due to impurity scattering. The considered Ti concentrations are 1.56, 3.13, 6.25, and 12.5 at.%. For comparison, the isotropic conductivity of silver is $\sim 63 \times 10^6$ Å/Vm.

Ti (at.%)	μ_d (cm^2/Vs)	Principal values (cm^2/Vs)	σ_d (10^6 Å/Vm)	Principal values (10^6 Å/Vm)
12.5	$\begin{pmatrix} 12.0 & -0.6 & 1.9 \\ -0.6 & 10.2 & -0.9 \\ 1.9 & -0.9 & 14.3 \end{pmatrix}$	$\begin{pmatrix} 10.0 \\ 10.9 \\ 15.6 \end{pmatrix}$	$\begin{pmatrix} 0.41 & -0.02 & 0.07 \\ -0.02 & 0.35 & -0.03 \\ 0.07 & -0.03 & 0.49 \end{pmatrix}$	$\begin{pmatrix} 0.34 \\ 0.37 \\ 0.53 \end{pmatrix}$
6.25	$\begin{pmatrix} 24.0 & -1.1 & 3.9 \\ -1.1 & 20.5 & -1.8 \\ 3.9 & -1.8 & 28.6 \end{pmatrix}$	$\begin{pmatrix} 20.1 \\ 21.8 \\ 31.2 \end{pmatrix}$	$\begin{pmatrix} 0.53 & -0.02 & 0.09 \\ -0.02 & 0.45 & -0.04 \\ 0.09 & -0.04 & 0.63 \end{pmatrix}$	$\begin{pmatrix} 0.44 \\ 0.48 \\ 0.69 \end{pmatrix}$
3.13	$\begin{pmatrix} 47.9 & -2.2 & 7.7 \\ -2.2 & 41.0 & -3.6 \\ 7.7 & -3.6 & 57.1 \end{pmatrix}$	$\begin{pmatrix} 40.1 \\ 43.5 \\ 62.4 \end{pmatrix}$	$\begin{pmatrix} 0.72 & -0.03 & 0.12 \\ -0.03 & 0.62 & -0.05 \\ 0.12 & -0.05 & 0.86 \end{pmatrix}$	$\begin{pmatrix} 0.60 \\ 0.66 \\ 0.94 \end{pmatrix}$
1.56	$\begin{pmatrix} 95.8 & -4.5 & 15.4 \\ -4.5 & 81.9 & -7.3 \\ 15.4 & -7.3 & 114.3 \end{pmatrix}$	$\begin{pmatrix} 80.2 \\ 87.1 \\ 124.7 \end{pmatrix}$	$\begin{pmatrix} 1.40 & -0.07 & 0.22 \\ -0.07 & 1.19 & -0.11 \\ 0.22 & -0.11 & 1.67 \end{pmatrix}$	$\begin{pmatrix} 1.17 \\ 1.27 \\ 1.82 \end{pmatrix}$

energy of the system. The band velocity $\vec{v}_n$ is the derivative of the energy $E_n(\vec{k})$ with respect to $\vec{k}$ divided by $\hbar$. Figure 9 shows the probability density distribution of the band velocity within $\pm k_B T$ of the Fermi level. We calculate velocity magnitudes and normalize the sum to 1. The distribution peaks at 2 Å/fs. The sum in Eq. (7) runs over 10 contributing bands at the Fermi level. Using Eq. (7), the conductivity is given by

$$\sigma_{\alpha\beta} = en\mu_{\alpha\beta}. \tag{8}$$

For the electron density n in Eq. (8), we use our previously estimated conduction electron density within the energy interval $-k_B T + E_F \leqslant E \leqslant E_F + k_B T$ (Table I).

We calculate the mobility and conductivity tensors of $Ti_xPt_{1-x}Si$ alloys for several Ti concentrations. Our calculations show that dense k-point meshes are crucial for accurate convergence of the conductivity tensor. We use a $10 \times 10 \times 12$ mesh for the $2 \times 2 \times 2$ simulation cell. Our results are listed in Table V. In this theory, no electron–phonon interaction or other types of interactions, besides the impurity scattering, are included. Thus, the result is not the absolute value for carrier mobility but rather a correction to the unperturbed absolute values. The total mobility and conductivity are calculated using the following expressions:

$$\frac{1}{\mu_{\text{tot}}} = \frac{1}{\mu_0} + \frac{1}{\mu_d} \rightarrow \mu_{\text{tot}} = \frac{\mu_d}{1 + \mu_d/\mu_0} \qquad \sigma_{\text{tot}} = en\mu_{\text{tot}} \tag{9}$$

The subscript d denotes the defect contribution calculated in this work, whereas subscript 0 denotes the absolute values without impurity scattering, for which we use the experimental value. We use $\sigma_0 \approx 3.3 \times 10^6$ Å/Vm[29] and $\mu_0 = \sigma_0/en_0 \approx 263.5$ cm^2/Vs.

In Fig. 10, we plot μ_{tot} and σ_{tot}. For μ_d and σ_d, we use the average of the principle values of our calculated tensors. The mobility and conductivity tensors for 1.56, 3.13, 6.25, and 12.5 at.% Ti are listed in Table V. Clearly, carrier mobility decreases with the increasing number of impurities. Contrary to what happens in doped semiconductors, the carrier density rises too slowly to offset the decrease in mobility, and conductivity decreases. However, for Ti concentrations below 0.5 at.%, the decrease in conductivity is less than 50% of that of bulk PtSi.

D. Thermodynamic stability and solubility limit

The question now arises of whether we can incorporate a sufficient amount of Ti on the Pt site in PtSi. Multicomponent silicides can be produced by depositing layers of metals on a Si substrate and subsequently heating until silicidation sets in. Typically, four reaction outcomes are distinguished: layer reversal, phase separation, solid solution, or ternary compound formation. These reactions can occur successively; for further details, refer to the work by Setton and van der Spiegel.[30] Because both Ti and Pt form silicide phases, we could, in principle, encounter formation of Ti_nSi, Pt_nSi, $PtTi_n$, their mixtures, or a ternary compound. To the simplest approximation, the alloy with the lowest formation energy would form first, followed by the alloy with the next highest formation energy, and so on. We calculate the heat of formation of PtTi, PtSi, and TiSi to be $\Delta H_{\text{PtTi}} = -1.72$ eV, $\Delta H_{\text{PtSi}} = -1.43$ eV, and $\Delta H_{\text{TiSi}} = -1.72$ eV, respectively, per formula unit. Considering just these three compounds

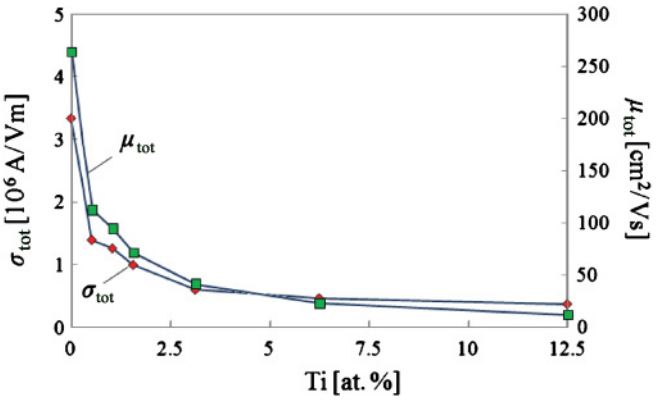

FIG. 10. (Color online) μ_{tot} and σ_{tot} for $\mu_0 \approx 263.5$cm^2/Vs and $\sigma_0 = \frac{1}{\rho_0} \approx 3.3 \times 10^6$ Å/Vm (from Ref. 27). μ_0 is obtained by dividing σ_0 by the elementary charge and carrier density. We find a monotonic degradation of conductivity for higher Ti concentrations.

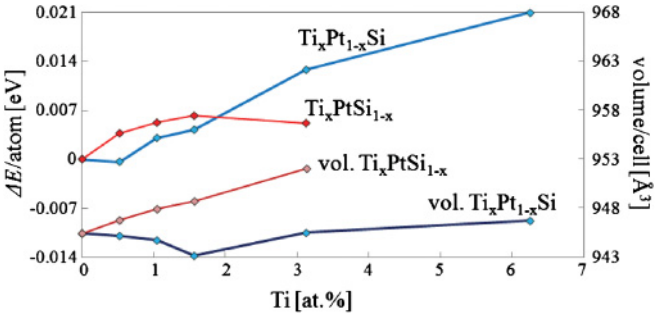

FIG. 11. (Color online) Formation energy and cell volume of the $Ti_xPt_{1-x}Si$ and Ti_xPtSi_{1-x} alloys. For low Ti concentrations (<1.8 at.%), Ti prefers to be mixed on the Pt site. Above this concentration, it tends to mix on the Si site.

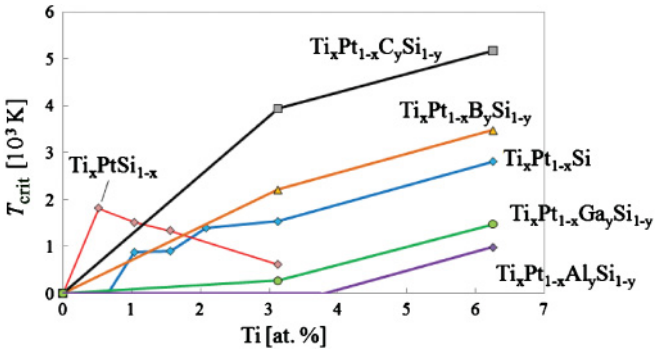

FIG. 12. (Color online) Solubility limit of Ti in different alloy compositions with and without codoping. While the x-fraction of Ti in the alloy is variable, the y-fraction (codopants) is fixed to 1/32 (corresponding to 1.56 at.%). The best codopant is Al, yielding stable alloys with up to 4 at.% Ti.

(not including higher-order silicides and titanides), the heats of formation indicate that upon heating the Ti/Pt/Si system, PtTi or TiSi would form first. $TiPt_n$ alloys are well known experimentally.[31–33] The formation of PtSi, $Ti_xPt_ySi_z$, or $Ti_xPt_{1-x}Si$ compounds would occur at a higher temperature.

The formation energy per formula unit of PtSi is higher than that of TiSi, suggesting that the substitution of Pt with Ti in PtSi would result in a stable $Ti_xPt_{1-x}Si$ alloy. By analyzing the changes in the internal energy after alloying, we identify the energetically preferred substitution site. The formation energy can be estimated by

$$PtSi + xTi \xrightarrow{\Delta E} Ti_xPt_{1-x}Si + xPt \tag{10}$$

and

$$PtSi + xTi \xrightarrow{\Delta E} Ti_xPtSi_{1-x} + xSi \tag{11}$$

for doping on the Pt and Si sites, respectively. The reaction energy in Eqs. (10) and (11) and the cell volume V of the alloys are plotted in Fig. 11 as functions of Ti concentration. The cell volume V is used later. Doping on a Pt site, we find a stable alloy with ∼0.5 at.% Ti. Above 0.5 at.%, the formation energy increases linearly with the Ti concentration. Doping on a Si site becomes energetically favorable over doping on a Pt site for more than ∼1.8 at.% Ti. We find a linear increase in the cell volume when doping on a Si site. However, mixing up to 2 at.% Ti on a Pt site "shrinks" the cell. Above 2 at.%, its volume starts increasing linearly. Interestingly, Ti's atomic radius is 5% larger than that of Pt yet produces a net volume decrease in cell size compared to PtSi.

To estimate Ti's solubility limit in PtSi, we calculate the change in free energy after alloying:

$$\Delta G = \Delta E + p\Delta V - TS_m. \tag{12}$$

Here, ΔE is the change in internal energy, $p\Delta V$ is the contribution due to the change in volume, and TS_m accounts for the change in entropy. For ΔE, we use the values calculated using the reactions in Eqs. (10) and (11). The $p\Delta V$ term is calculated from the change in the volume after alloying multiplied by $p = 1$ atm. The entropic contribution in Eq. (12) is estimated using a simple theory of ideal binary mixtures:

$$S_m = -k_B \ln\left(\frac{N_1! \times N_2!}{N_{\text{total}}!}\right). \tag{13}$$

Assuming Ti is substituted for either Pt or Si, N_1 is the number of Ti atoms, $N_2 = N_{\text{Pt/Si}} - N_1$ is the number of remaining Pt or Si atoms, and $N_{\text{tot}} = N_1 + N_2$. The entropic term is stabilizing the alloys above the "critical temperature" when ΔG becomes negative. The critical temperature is determined by the condition $\Delta G = 0$ in Eq. (12):

$$T_{\text{crit}} = \frac{\Delta E + p\Delta V}{S_m}, \tag{14}$$

where the ΔE, $p\Delta V$, and S_m terms depend on the Ti concentration. Therefore, plotting Eq. (14) as a function of the Ti concentration shows the solubility limit of Ti in PtSi at a particular critical temperature.

Our results for T_{crit} are summarized in Table I and Fig. 12. Up to ∼0.7 at.% Ti mixes on the Pt site. Above ∼0.7 at.%, the solubility limit of Ti increases linearly with temperature. At 500K, up to ∼0.9 at.% Ti can be mixed in PtSi (substituting Pt), while at PtSi's congruential melting temperature of 1500 K, only up to ∼2 at.% Ti can be mixed on the Pt site. This can be traced to a chemical difference manifested in the Pt–Si and Ti–Si bond lengths. We find that the nearest neighbor distance in TiSi is 2.6 Å, while in PtSi it is 2.4 Å, deviating by 7.5%. Thus, alloying introduces significant local stress. However, up to ∼3 at.% Ti can be mixed on the Si site at 500 K. We have also considered a possibility of Ti clustering and find that it is not energetically preferable. To obtain a notable gain in carrier density with increasing Ti concentration, 1.8 at.% and more Ti should mix on the Pt site. Thus, in Sec. IV, we analyze possible routes to increase the Ti solubility limit at low temperature and to stabilize $Ti_xPt_{1-x}Si$ versus Ti_xPtSi_{1-x} alloys.

IV. CODOPING WITH BORON, CARBON, GALLIUM, AND ALUMINUM

We can think of several ways to increase the solubility of Ti in PtSi. The parameters in Eq. (14) that control the solubility limit are the formation energy ΔE, the cell volume, and the entropy of mixing. The solubility limit increases when

TABLE VI. Reaction energy, carrier concentration, and critical temperature of $Ti_2Pt_{30}XSi_{31}$ (3.13 at.% Ti) and $Ti_4Pt_{28}XSi_{31}$ (6.25 at.% Ti) alloys. Negative critical temperature indicates stable alloys as the numerator in Eq. (14) becomes negative. Codoping with Ga and Al yields a large increase in the solubility limit at a given temperature compared to that of pure $Ti_xPt_{1-x}Si$ alloys.

	3.13 at.% Ti			6.25 at.% Ti		
X	ΔE (eV/atom)	T_{crit} (K)	n (10^{20} cm^{-3})	ΔE (eV/atom)	T_{crit} (K)	n (10^{20} cm^{-3})
–	0.013	1532	9.4	0.021	2809	13.8
B	0.029	2211	10.0	0.042	3477	11.1
C	0.051	3933	8.3	0.063	5168	15.1
Ga	0.003	269	10.9	0.018	1474	11.9
Al	−0.004	0	11.3	0.012	983	12.7

either the formation energy or the cell volume decrease, the entropy of mixing increases, or any combination of these three possibilities occurs. Our smallest $2 \times 2 \times 2$ cell for 1.56 at.% Ti is 2.3 Å^3 smaller than bulk PtSi. Our largest $2 \times 2 \times 2$ cell for 3.13 at.% Ti is 6.6 Å^3 larger than PtSi. Assuming pressure of 1 atm, the $p\Delta V$ term in Eq. (14) ranges between -1.4×10^{-3} and 4.1×10^{-3} meV, less than 0.07% of the smallest energy difference we calculate using Eqs. (10) and (11). Thus, the $p\Delta V$ contribution is too small on the scale of ΔE to make a significant difference in an alloy's stability [Eq. (14)]. Instead, we consider codoping TiPtSi with boron, carbon, gallium, and aluminum ions (denoted as X later on) to increase the entropic contribution and hopefully reduce ΔE. We use alloys with 3.13 and 6.25 at.% concentrations of Ti. First, we consider doping Ti on the Pt site while codoping with one of the proposed elements. For the energetically preferred codopant, we later reevaluate the preferred doping site of Ti.

We use a $2 \times 2 \times 2$ simulation cell and substitute one x atom on either the Pt or the Si site. Despite the large difference in the atomic radii of our codopants and Pt and Si, we find that all proposed codopants prefer to mix substitutionally on the Si site. The formation energy of $Ti_xPt_{1-x}X_ySi_{1-y}$ is estimated using the following reactions:

$$32\mathrm{PtSi} + 2\mathrm{Ti} + X \xrightarrow{\Delta E} \mathrm{Ti_2Pt_{30}}X\mathrm{Si_{31}} + 2\mathrm{Pt} + \mathrm{Si} \quad (15)$$

and

$$32\mathrm{PtSi} + 4\mathrm{Ti} + X \xrightarrow{\Delta E} \mathrm{Ti_4Pt_{28}}X\mathrm{Si_{31}} + 4\mathrm{Pt} + \mathrm{Si} \quad (16)$$

for 3.13 and 6.25 at.% Ti, respectively. The formation energy for all codopants, along with the carrier density at the Fermi level, is summarized in Table VI. In all alloys, the carrier density at the Fermi level is increased compared to that of bulk PtSi. While codoping with boron and carbon increases the formation energy of the alloy, gallium or aluminum lowers the formation energy drastically. We find the largest decrease in formation energy when using Al as a codopant and identify a marginally stable $Ti_xPt_{1-x}Al_ySi_{1-y}$ alloy with 3.12 at.% Ti.

For this alloy, we also consider introducing Ti on a Si site to identify the preferences of the mixing site. The formation energy is calculated from

$$32\mathrm{PtSi} + 2\mathrm{Ti} + \mathrm{Al} \xrightarrow{\Delta E} \mathrm{Ti_2AlPt_{32}Si_{29}} + 3\mathrm{Si}. \quad (17)$$

It is −10 meV/atom, 6.5 meV/atom smaller than when mixing Ti on the Pt site. The energy difference is very small, suggesting that Ti will occupy both the Pt and the Si sites with equal probability. Thus, independent of the site with which Ti mixes, the alloy's stability can be increased through codoping with Al.

Using the formation energy calculated in Eqs. (15) and (16) in Eq. (14), we recalculate the solubility limit of titanium. For the entropic contribution, we assume that Ti only mixes on the Pt site while the codopant x only mixes on the Si site. The entropy of mixing is then 1.3×10^{-5} and 1.2×10^{-5} eV/K in $Ti_2Pt_{30}XSi_{31}$ (3.13 at.% Ti) and $Ti_4Pt_{28}XSi_{31}$ (6.25 at.% Ti), respectively. The critical temperatures are summarized in Table VI, and the solubility limit of Ti is shown in Fig. 12. Although B and C do not improve the solubility, Ga and Al increase it significantly when compared to both $Ti_xPt_{1-x}Si$ and Ti_xPtSi_{1-x}. At room temperature, more than 4 at.% Ti can be mixed in PtSi when codoping with Al. A linear interpolation between $Ti_2Pt_{30}AlSi_{31}$ and $Ti_4Pt_{28}AlSi_{31}$ suggests a 1.5-fold increase in carrier density for 4 at.% Ti compared to bulk PtSi.

So far, we have only considered reactions between PtSi and other elements. To analyze the possible alloy decomposition, we consider reactions competing with the formation of $Ti_xPt_{1-x}X_ySi_{1-y}$. To do so, we calculate the reaction energy of two reactions,

$$\mathrm{Ti_2Pt_{30}}X\mathrm{Si_{31}} \xrightarrow{\Delta E} 30\mathrm{PtSi} + \mathrm{TiSi} + \mathrm{Ti}X \quad (18)$$

and

$$\mathrm{Ti_4Pt_{28}}X\mathrm{Si_{31}} \xrightarrow{\Delta E} 28\mathrm{PtSi} + 3\mathrm{TiSi} + \mathrm{Ti}X, \quad (19)$$

for 3.12 and 6.25 at.% Ti, respectively. The energies for the PtSi, TiSi, and TiX are extracted from the respective bulk calculations. To keep the analysis simple, we do not consider reactions with higher-order silicides such as $PtSi_2$ or $TiSi_2$. Negative reaction energy indicates thermodynamically preferred decomposition. We find negative energy in all cases except when codoping a 3.13 at.% alloy with aluminum. In this case, the reaction energy is 8.2 meV/atom. Unlike other alloys, this one does not have a thermodynamic preference to decompose into a mixture of binary intermetallics PtSi, TiSi, and TiAl.

V. CONCLUSIONS

We use theoretical band engineering to analyze and find ways to control the electrical properties of the technologically important contact material PtSi. We find that alloying PtSi with Ti may considerably increase the number of carriers. The improvement comes from the introduction of titanium d

states near the Fermi level. Moreover, we find that although doping with Ti lowers the WF of PtSi by as much as 0.45 eV, the SBH to Si is rather insensitive to this change. Using a combination of density functional theory and Boltzmann transport formalism, we show that the increase in carrier concentration is accompanied by alloy scattering that adversely affects conductivity despite a significant increase in the number of carriers. For doping concentrations below 0.5 at.% the conductivity decreases by less than 50% of that of bulk PtSi. The thermodynamic analysis indicates that under equilibrium conditions at room temperature, only 0.7 at.% Ti can be mixed in PtSi by substituting for Pt. The low solubility is attributed to strain caused by Ti in the PtSi lattice. To achieve higher doping concentrations, we suggest codoping PtSi with gallium or aluminum. While aluminum is best, both increase Ti solubility at room temperature to more than 3 at.%.

ACKNOWLEDGMENTS

We thank C. Murray of IBM Research for stimulating discussions. This work was supported by the National Science Foundation under Grant No. DMR1006725 and the Texas Advanced Computing Center.

*demkov@physics.utexas.edu

[1] S. Yhang and M. Ostling, CRC Crit. Rev. Solid State Mater. Sci. **28**, 1 (2003).
[2] C. Detavernier, A. S. Ozcan, J. Jordan-Sweet, E. A. Stach, J. Tersoff, F. M. Ross, and C. Lavoie, Nature (London) **426**, 641 (2003).
[3] C. Detavernier and C. Lavoie, Appl. Phys. Lett. **84**, 3549 (2004).
[4] E. H. Rhoderick and R. H. Williams, *Metal–Semiconductor Contacts (Electrical & Electronic Engineering Monographs)*, 2nd ed. (Oxford Univ. Press, New York, USA, 1988).
[5] J. E. Klepeis, O. Beckstein, O. Pankratov, and G. L. W. Hart, Phys. Rev. B **64**, 155110 (2001).
[6] N. Franco, J. E. Klepeis, C. Bostedt, T. Van Buuren, C. Heske, O. Pankratov, T. A. Callcott, D. L. Ederer, and L. J. Terminello, Phys. Rev. B **68**, 045116 (2003).
[7] O. Beckstein, J. E. Klepeis, G. L. W. Hart, and O. Pankratov, Phys. Rev. B **63**, 134112 (2001).
[8] M. K. Niranjan, S. Zollner, L. Kleinman, and A. A. Demkov, Phys. Rev. B **73**, 195332 (2006).
[9] H. Bentmann, A. A. Demkov, R. Gregory, and S. Zollner, Phys. Rev. B **78**, 205302 (2008).
[10] V. W. Chin, M. A. Green, and J. W. V. Storey, Solid-State Electron. **36**, 1107 (1993).
[11] E. J. Graeber, R. J. Baughman, and B. Morossin, Acta Crystallogr. **29**, 1991 (1973).
[12] D. Vanderbilt, Phys. Rev. B **41**, 7892 (1990).
[13] G. Kresse and J. Hafner, Phys. Rev. B **47**, 558 (1993).
[14] G. Kresse and J. Furthmüller, Comput. Mater. Sci. **6**, 15 (1996).
[15] G. Kresse and J. Furthmüller, Phys. Rev. B **54**, 11169 (1996).
[16] G. Kresse and J. Hafner, J. Phys. Condens. Matter. **6**, 8245 (1994).
[17] G. Kresse and D. Joubert, Phys. Rev. B **59**, 1758 (1999).
[18] H. J. Monkhorst and J. D. Pack, Phys. Rev. B **13**, 5188 (1976).
[19] W. A. Harrison, *Elementary Electronic Structure*, revised ed. (World Scientific Publishing, Singapore, 2004).
[20] V. Heine, Phys. Rev. A **138**, 1689 (1965).
[21] W. Mönch, *Electronic Structure of Metal–Semiconductor Contacts* (Kluwer, Dordrecht, 1990).
[22] J. Robertson and B. Falabretti, J. Appl. Phys. **100**, 014111 (2006).
[23] J. Tersoff, Phys. Rev. B **30**, 4874 (1984).
[24] M. Elices and F. Yndurain, J. Phys. C Solid State Phys. **5**, L146 (1972).
[25] S. M. Sze, *Physics of Semiconductor Devices* (Wiley, New York, 1981).
[26] H. Bruus and K. Flensburg, *Many-Body Quantum Theory in Condensed Matter Physics: An Introduction* (Oxford University Press, New York, USA, 2004).
[27] G. Mahan, *Many-Particle Physics*, 2nd ed. (Plenum, New York, 1990).
[28] M. H. Evans, X.-G. Zhang, J. D. Joannopoulos, and S. T. Pantelides, Phys. Rev. Lett. **95**, 106802 (2005).
[29] P. I. Gaiduk and A. N. Larsen, Appl. Phys. A **53**, 167 (1991).
[30] M. Setton and J. van der Spiegel, Thin Sol. Films **156**, 351 (1988).
[31] L. S. Hung and J. W. Mayer, J. Appl. Phys. **60**, 1002 (1986).
[32] T. Biggs, L. A. Cornish, M. J. Witcomb, and M. B. Cortie, J. Alloys Compd. **375**, 120 (2004).
[33] R. Hung, Q. Z. Hong, and J. W. Mayer, J. Appl. Phys. **63**, 1749 (1988).